Studying triangle singularity through spin observables

Ke Wang,[1,2] Shao-Fei Chen,[1,2] and Bo-Chao Liu[1,2,*]

[1]*MOE Key Laboratory for Nonequilibrium Synthesis and Modulation of Condensed Matter, School of Physics, Xi'an Jiaotong University, Xi'an 710049, China*

[2]*Institute of Theoretical Physics, Xi'an Jiaotong University, Xi'an 710049, China*

(Received 26 June 2022; accepted 7 November 2022; published 28 November 2022)

In this work, we study the spin density matrix element ρ_{00} of the ϕ in the decay $J/\psi \to \eta\pi\phi$. In previous studies, a band around 1.4 GeV on the $\pi^0\phi$ distribution in Dalitz plot was reported by the BESIII Collaboration. This structure may be caused by the production of a resonance or the triangle singularity mechanism. We find that the predictions of the spin density matrix elements of the final ϕ based on these mechanisms show distinct features. Thus the measurement of the spin density matrix elements of the ϕ in this reaction may offer an alternative way to study the triangle singularity and to clarify the reaction mechanisms, i.e., resonance production or kinematic effects. This work also shows the potential of spin observables in studying kinematic singularities.

DOI: 10.1103/PhysRevD.106.094032

I. INTRODUCTION

The studies on the hadron spectrum offer the platform to test our knowledge of quantum chromodynamics (QCD) in the nonperturbative regime, which is important for understanding the strong interactions. In recent years, owing to a large amount of new experimental results on particle reactions and resonances there have been significant progress in the study of the hadron spectrum. A large number of new states were found, which usually show as peaks or dips in the invariant mass spectrum of final particles. While a peak in the invariant mass spectrum is not necessarily caused by a resonance. It also can be produced by kinematic effects. In fact, some of the new states are interpreted as threshold cusps and/or triangle singularities [1–9]. Since these kinematic effects may show similar features as resonances, it is then important to find some ways to distinguish the kinematic singularities from genuine resonances.

Besides the interests in clarifying the nature of the observed structures in experiments, triangle singularity (TS) mechanism may also play an essential role in understanding some important puzzles. Some remarkable examples can be found in relevant studies in J/ψ decays. In 2012, BESIII Collaboration reported the observation of abnormally large isospin-breaking effects in $J/\psi \to \gamma\eta(1405/1475) \to \gamma + 3\pi$ [10], which, however, could be understood by considering the important roles of the TS mechanism via the intermediate $K^*\bar{K} + \text{c.c.}$ rescatterings in this decay. Furthermore, it was also argued that the TS mechanism could be crucial for understanding the nature of η resonances [11,12] and the productions and decays of light axial vector mesons [13] in J/ψ decays. Even though the TS mechanism may play important roles in the physical processes mentioned above, further experimental evidences are still needed to identify its contribution. Up to now, most studies on the TS mechanism mainly concentrate on its effects in the invariant mass spectrum. In this work, we hope to show that the TS mechanism may also cause significant spin effects and in some cases spin observables are helpful for identifying its contributions. Here we will concentrate on the reaction $J/\psi \to \eta\pi\phi$. In Ref. [14], it was argued that if considering the contributions from a set of $K^*K\bar{K}$ triangle diagrams [Fig. 1(a)] a peak around 1.4 GeV in the $\pi^0\phi$ invariant mass distribution can be produced in the $J/\psi \to \eta\pi\phi$ reaction, which fits well with the recent measurement on this reaction by BESIII Collaboration [15]. Of course, the peak observed by experiment can also be interpreted by considering the production of a resonance [Fig. 1(c)]. In Ref. [14], the authors suggested that by checking whether the structure around 1.4 GeV persists for the K^+K^- invariant mass away from the ϕ mass region one could distinguish these two models. Later, the authors in Ref. [13] argued that the decay could also proceed with the production of $h_1(1415)$ at first and then $h_1(1415)$ decaying to $\pi\phi$ through the same triangle diagram [Fig. 1(b)]. Both the models in Refs. [13,14] concern the TS mechanism, and we call them the TS models to distinguish from the resonance model

*liubc@xjtu.edu.cn

Published by the American Physical Society under the terms of the Creative Commons Attribution 4.0 International license. Further distribution of this work must maintain attribution to the author(s) and the published article's title, journal citation, and DOI. Funded by SCOAP³.

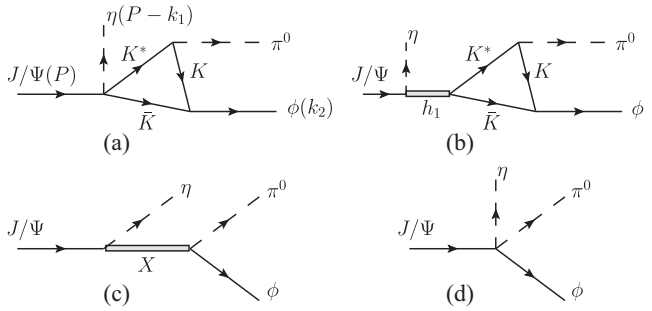

FIG. 1. Feynman diagrams for the $J/\psi \to \eta\pi\phi$ reaction.

where a resonance is produced and decays without significant rescattering effects. In this work, we will show that it is possible to distinguish these two kinds of models by measuring the spin density matrix elements (SDMEs) of the final ϕ.

This paper is organized as follows. In Sec. II, the theoretical framework and ingredients are presented. In Sec. III, the numerical results are presented with some discussions. Finally, the paper ends with a short summary in Sec. IV.

II. MODEL AND FORMALISM

As mentioned in Sec. I, a peak structure being around 1.4 GeV in the $\pi\phi$ invariant mass spectrum was found in the reaction $J/\psi \to \eta\pi\phi$ [15]. This peak may be caused by a resonance (resonance model), e.g., C(1480) [16,17]/ $h_1(1415)$ [18–20], or triangle diagrams involving $K^*K\bar{K}$ intermediate states (TS model) as discussed in Refs. [13,14]. The Feynman diagrams for the TS and resonance models can be depicted in Fig. 1. To calculate these Feynman diagrams, the Lagrangian densities for the involved vertices are needed. For the triangle diagrams, we basically follow the formalism in Ref. [14], where the triangle diagrams were calculated. As shown in Ref. [14], the amplitudes for Fig. 1(a) can be presented as

$$\mathcal{M}_i = ig\epsilon^{\mu}_{J/\psi}\epsilon^{*\nu}_{\phi}\int\frac{d^4q}{(2\pi)^4}\frac{[-g_{\mu\lambda}+(q+k_1)_\mu(q+k_1)_\lambda/m^2_{K^*_{id}}](q+2k_2-k_1)^\lambda(2q+k_2)\nu}{(q^2-m^2_{K_{id}}+i\epsilon)[(q+k_1)^2-m^2_{K^*_{id}}+i\epsilon][(q+k_2)^2-m^2_{K_{id}}+i\epsilon]} \equiv ig\epsilon^{\mu}_{J/\psi}\epsilon^{*\nu}_{\phi}\mathcal{M}^i_{\mu\nu}, \quad (1)$$

where the index $i = C(N)$ denotes the amplitudes corresponding to the process with the charged (neutral) intermediate particles and g is a constant. The concrete expressions of $\mathcal{M}^i_{\mu\nu}$ and meanings of parameters can be found in Ref. [14]. By summing the charged and neutral loop amplitudes, with including the appropriate coefficients, the total amplitude can be presented as

$$\mathcal{M} = 2(\mathcal{M}_C - \mathcal{M}_N). \quad (2)$$

For the amplitude of Fig. 1(b), where $h_1(1415)$ is produced at first, the total amplitude can also be written as Eq. (2) but with the $\mathcal{M}_{i=C(N)}$ being replaced by [13,18]

$$\mathcal{M}_i \equiv i\frac{g'\epsilon_{J/\psi,\rho}(-g^{\rho\mu}+k_1^\rho k_1^\mu/k_1^2)\epsilon^{*\nu}_{\phi}\mathcal{M}^i_{\mu\nu}}{k_1^2-m^2_{h_1}+im_{h1}\Gamma_{h_1}}, \quad (3)$$

where the $\mathcal{M}^i_{\mu\nu}$ is defined in Eq. (1) and g' represents the coupling constant.

To calculate the tree diagram in the case of the C(1480) production, we need to consider the process represented by Fig. 1(c) with taking X as C(1480) ($I = 1$, $J^{PC} = 1^{--}$) [16,17]. The effective Lagrangians for the $J/\psi X\eta$ and $X\pi\phi$ vertices are adopted as [21]

$$\mathcal{L}_{VVP} = g_V\varepsilon^{\mu\nu\alpha\beta}\partial_\mu V_\nu\partial_\alpha V_\beta P, \quad (4)$$

where V denotes the field of a vector meson (J/ψ or ϕ), and P denotes the field of a pseudoscalar meson (η or π). Note that isospin invariance needs not to be considered for the $J/\psi X\eta$ or $X\pi\phi$ vertex depending on the isospin of X being 1 or 0, respectively, because isospin conservation is violated in this decay. The amplitude for this tree diagram can then be obtained as

$$-i\mathcal{M}_{C(1480)} = g_C\varepsilon_{\mu\nu\alpha\beta}p^\mu_\phi\phi^{*\nu}p^\alpha_C G_1^{\beta b}(p_C)\varepsilon_{abcd}p^a_C p^c_\psi\psi^d, \quad (5)$$

where g_C represents the product of coupling constants in this process, and the $G_1^{\mu\nu}$ is taken as

$$G_1^{\mu\nu}(p_X) = \frac{-g^{\mu\nu}+\frac{p^\mu_X p^\nu_X}{p^2_X}}{p^2_X-m^2_X+im_X\Gamma_X}. \quad (6)$$

For the mass and width of the C(1480), we adopt $m_{C(1480)} = 1480$ and $\Gamma_{C(1480)} = 130$ MeV [16,17].

For the case that the intermediate state X is the $h_1(1415)$, the Feynman diagram for the process can also be presented by Fig. 1(c) with taking X as $h_1(1415)$. Since h_1 has quantum numbers $I = 0$ and $J^{PC} = 1^{+-}$, the effective Lagrangian for the $J/\psi h_1\eta$ and $h_1\phi\pi$ vertices can be written as [22,23]

$$\mathcal{L}_{AVP} = g_A(\mathcal{L}_a\cos\theta + \mathcal{L}_b\sin\theta), \quad (7)$$

$$\mathcal{L}_a = A^\mu(\partial_\mu V_\nu - \partial_\nu V_\mu)\partial^\nu P, \tag{8}$$

$$\mathcal{L}_b = \partial^\mu A^\nu(\partial_\mu V_\nu - \partial_\nu V_\mu)P, \tag{9}$$

where V denotes J/ψ or ϕ field, P denotes π or η field and A represents h_1 field. The g_A and θ represent the coupling constant and mixing angle.

Then the corresponding amplitude for Fig. 1(c) can be obtained as

$$\begin{aligned} -i\mathcal{M}_h = {} & g_h G_1^{\mu a}(p_{h_1}), \\ & \times (p_{\phi\mu}\phi_\nu - p_{\phi\nu}\phi_\mu)(p_\pi^\nu \cos\theta_\pi + p_{h_1}^\nu \sin\theta_\pi), \\ & \times (p_{\psi a}\psi_b - p_{\psi b}\psi_a)(p_\eta^b \cos\theta_\eta - p_{h_1}^b \sin\theta_\eta), \end{aligned} \tag{10}$$

where θ_η and θ_π represent the mixing angles in the Lagrangians of the $J/\psi h_1\eta$ and $h_1\phi\pi$ vertices, respectively. The mass and width of h_1 can be taken from PDG book [19] as $m_{h_1} = 1416$ and $\Gamma_{h_1} = 90$ MeV.

III. THE SPIN DENSITY MATRIX ELEMENTS

With the amplitudes given above, the spin density matrix elements of the final ϕ in the $J/\psi \to \phi\eta\pi$ reaction can be calculated. Since the initial J/ψ considered in this work is produced in e^+e^- collisions, we choose the polarization axis of J/ψ along z axis, which is defined as the beam direction of e^+ or e^-. In this case, the magnetic quantum numbers of the J/ψ only takes the values $m = \pm 1$ [24]. For the final ϕ, we shall consider its helicity states, i.e., choosing its polarization axis along its momentum direction, in the c.m. frame of the $\pi^0\phi$ system. The spin density matrix element ρ_{00} of the ϕ (denoted as ρ_{00}^ϕ) as a function of the $\pi^0\phi$ invariant mass in the $\pi^0\phi$ rest frame is defined as

$$\rho_{00}^\phi(m_{\pi^0\phi}) = \frac{\int d\Omega_\eta d\Omega_{\pi^0} \sum_m \mathcal{M}_{m,\lambda=0}\mathcal{M}^*_{m,\lambda'=0}}{\int d\Omega_\eta d\Omega_{\pi^0} \sum_{m,\lambda''} |\mathcal{M}_{m,\lambda''}|^2}, \tag{11}$$

where $m(=\pm 1)$ represents the z component of the total angular momentum of J/ψ and λ, λ' and λ'' are the helicities of the final ϕ. The ρ_{00}^ϕ can be extracted from the angular distribution of K or $\bar{K}$ in $\phi \to K\bar{K}$ through [25–27]

$$W(\cos\theta) \sim \frac{3}{2}\left[\rho_{00}^\phi \cos^2\theta + \frac{1}{2}(1-\rho_{00}^\phi)\sin^2\theta\right], \tag{12}$$

where θ is defined in the conventions of the helicity system.

TABLE I. Parameters for resonance models.

Model	Resonance	J^{PC}	Mass(GeV)	Width(GeV)	θ_π
I	$C(1480)$	1^{--}	1.480	0.13	⋯
IIA	$h_1(1415)$	1^{+-}	1.416	0.09	$\pi/4$
IIB	$h_1(1415)$	1^{+-}	1.416	0.09	$3\pi/4$

IV. RESULT AND DISCUSSION

As we know, both the kinematic singularity and genuine resonance state can result in a structure in the invariant mass spectrum. Therefore, it is interesting and important to find some other observables to distinguish these two mechanisms. In this section, we shall study the dependence of the SDME ρ_{00}^ϕ on the invariant mass spectrum $m_{\pi\phi}$ considering different mechanisms, and then discuss the possibility of distinguishing various mechanisms using this observable. For the purpose of this work, it is helpful to firstly study the features of the ρ_{00}^ϕ induced by the mechanisms shown in Fig. 1 individually. In doing so, the coupling constants are irrelevant. Therefore, we just set all the coupling constants as 1, and the possible effects from background contribution will be discussed later. For reader's convenience, the parameters for the resonance models are collected and listed in Table I.

In the case of the resonance production process with taking $X = C(1480)$ (Model I), the SDME ρ_{00}^ϕ is 0 as shown by the black dotted line in Fig. 2. This means that the final ϕ meson can only be in the helicity states with $\lambda = \pm 1$. This results from the properties of the $C\pi\phi$ (V-V-P coupling) vertex, which is discussed in detail in Appendix B.

In the case that X is the $h_1(1415)$, to calculate the amplitude we have to fix the values of the mixing angles θ_η and θ_π in the Lagrangians first. In general, the mixing

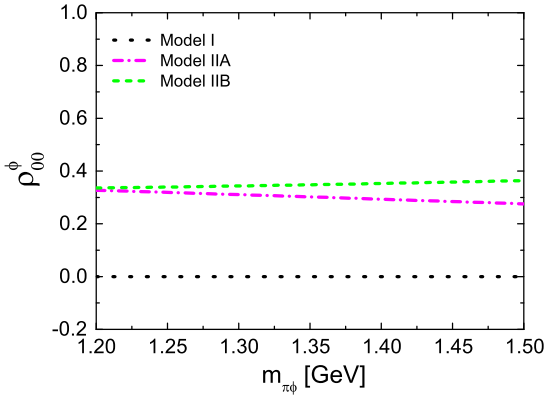

FIG. 2. The obtained ρ_{00}^ϕ for the tree diagrams. The dotted (black), short-dash-dotted (magenta), and short-dashed (green) lines represent the results of the $C(1480)$ production (Model I), $h_1(1415)$ production with taking $\theta_\pi = \pi/4$ (Model IIA) and $\theta_\pi = 3\pi/4$ (Model IIB), respectively.

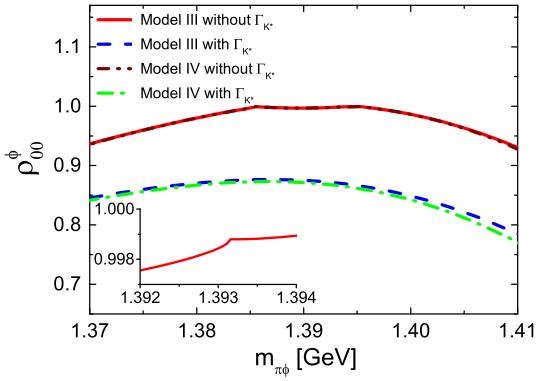

FIG. 3. The obtained ρ_{00}^{ϕ} for Model III and Model IV near the TS with and without considering the width of K^*.

angles should be determined by fitting the experimental data. Unfortunately, up to now the information about these angles is still absent. In our calculations, we find that the value of the ρ_{00}^{ϕ} is independent of the θ_η. On the other hand, the value of θ_π is relevant to the ρ_{00}^{ϕ}. If we take $\theta_\pi = \pi/4$ (Model IIA), which leads to a mixing of S-wave and D-wave couplings, the value of the ρ_{00}^{ϕ} is about 0.30 (the magenta short-dash-dotted line in Fig. 2). If we take $\theta_\pi = 3\pi/4$ (Model IIB), the $\mathcal{L}_{h_1\phi\pi}$ describes the S-wave coupling, and the value of ρ_{00}^{ϕ} is about 0.35 (the green short-dashed line in Fig. 2). In a general case, the mixing angles can be arbitrary and control the relative importance of the S-wave and D-wave couplings. However, we find that the D-wave contribution is suppressed compared to the S-wave contribution, and the mixing angle only has minor effects on the value of the ρ_{00}^{ϕ} except for taking θ_π at some special value.[1] Therefore, in the $h_1(1415)$ production case we conclude that the ρ_{00}^{ϕ} tends to be a relatively small value.

In Refs. [13,14], the authors have analyzed the $J/\psi \to \eta\pi^0\phi$ reaction by considering the triangle diagrams Fig. 1(a) (Model III) [14] or Fig. 1(b) (Model IV) [13] and shown that those diagrams can cause a peak around 1.4 GeV in the $\pi^0\phi$ invariant mass distribution. In fact, there are two kinds of singularities which are relevant [28]. One is the normal two-body threshold cusp (TBTC), and the other is the triangle singularity. Using the parameters of the particles from the PDG book [19], the TBTC and TS for the diagrams with the charged intermediate states are located at 1.3853 and 1.3857 GeV, respectively. And for diagrams with the neutral intermediate states they are located at 1.3931 and 1.3952 GeV, respectively. The SDME ρ_{00}^{ϕ} for the triangle diagrams (Model III and IV) near the TS has been studied with or without considering the width of the K^* in the loop in Fig. 3. In all TS models, the ρ_{00}^{ϕ} is always larger than 0.75. When neglecting the K^* width, there are two peaks in the distribution of ρ_{00}^{ϕ} versus the $\pi^0\phi$ invariant mass. At the peaks, the ρ_{00}^{ϕ} approaches 1. After including the K^* width effects, the distribution of ρ_{00}^{ϕ} only has one relatively wide peak. At the same time, the value of ρ_{00}^{ϕ} will decline to 0.77–0.88.

The relatively large value of ρ_{00}^{ϕ} induced by the triangle diagrams may be ascribed to the properties of the $K\bar{K}\phi$ vertex. Taking Fig. 1(a) as an example, if the three-momenta of K and ϕ are collinear, a large value of ρ_{00}^{ϕ} will be obtained as discussed in Appendix B. Since the considered invariant mass $m_{\pi\phi}$ in Fig. 3 is near the $\bar{K}K^*$ threshold, the magnitude of the three momentum of the $\bar{K}$ is close to zero when the intermediate states K^* and $\bar{K}$ in the loop are on shell. In this case, the three-momenta of K and ϕ are approximately collinear. Since it is expected that when the intermediate states are on shell the amplitude will get a relatively large value, the case discussed above gives the main contribution in the loop integral [18]. Thus the density matrix element ρ_{00}^{ϕ} tends to have a large value. This property also leads to the cusp at TBTC (see the inset plot in Fig. 3). Based on the same logic, without considering the K^*'s width the ρ_{00}^{ϕ} should approach 1 at TS, where the three intermediate particles are on shell and moving collinearly [28].

On the other hand, when the value of $m_{\pi\phi}$ moves away from the $\bar{K}K^*$ threshold, the collinear condition does not hold anymore. Therefore, the value of ρ_{00}^{ϕ} decreases as $m_{\pi\phi}$ departing from the locations of TS and TBTC. In Fig. 4, we show the SDME ρ_{00}^{ϕ} in a wider range of $m_{\pi\phi}$. No matter whether the width of K^* is considered, the ρ_{00}^{ϕ} distribution shows a wide peak, which is peaked at around

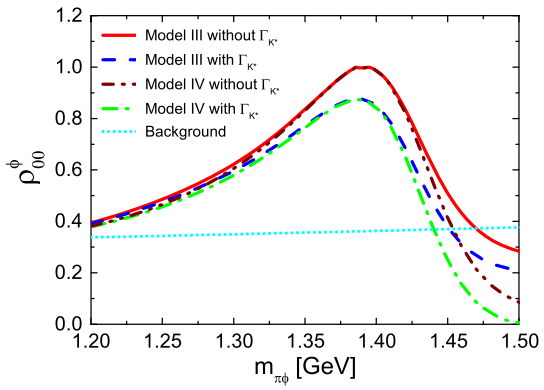

FIG. 4. The obtained ρ_{00}^{ϕ} for Model III and Model IV in a wider range of $m_{\pi\phi}$ with and without considering the width of K^*. The results for background contribution is also shown for comparison.

[1]In fact, we find that when the $h_1\pi\phi$ coupling has the form $h_1^{\mu}\partial_\mu\phi_\nu\partial^\nu\pi$ the ρ_{00}^{ϕ} can approach 1. But this only happens in a very small parameter space of the θ_π, otherwise the dependence of the ρ_{00}^{ϕ} on the θ_π is rather weak. So in this work we ignore the possibility that the $h_1\pi\phi$ vertex has this special coupling, which can certainly be verified by future studies on the $h_1\pi\phi$ coupling.

$m_{\pi\phi} = 1.39$ GeV. Comparing with the results of the resonance models in Fig. 2, it is clear that the ρ_{00}^{ϕ} show distinct features for the various models which all can explain the peak at around 1.4 GeV in the $\pi^0\phi$ invariant mass distribution. Therefore, the ρ_{00}^{ϕ} has the potential to clarify whether the structure in the invariant mass spectrum is caused by genuine resonance or by the TS mechanism.

Concerning the ρ_{00}^{ϕ} focused in this work, the main discrepancies between Models III and IV appear at higher $m_{\pi\phi}$. In fact, if one looks at the structures of the amplitudes of the two models, the main difference originates from the term $\frac{p^\mu p^\nu}{p^2}$ in the propagator of h_1 in Model IV [see Eq. (3)]. Note that the denominator of the h_1 propagator is canceled in the calculations of the ρ_{00}^{ϕ} [see Eq. (11)]. The presence of the $\frac{p^\mu p^\nu}{p^2}$ term guarantees that the total angular momentum of the $\pi\phi$ system is 1. While, at lower $m_{\pi\phi}$ the dominance of the S-wave component of the final $\pi\phi$ and intermediate $\bar{K}K^*$ systems automatically enforce that the total angular momentum of the $\pi\phi$ system is 1. Therefore, the two models give similar results. At higher $m_{\pi\phi}$, the $\frac{p^\mu p^\nu}{p^2}$ term starts to play a more important role, and the difference between the two models become evident. Numerically, if one calculates the contributions from the $-g_{\mu\nu}$ and $\frac{p^\mu p^\nu}{p^2}$ terms individually, it can be found that the $-g_{\mu\nu}$ term gives the dominant contribution at lower $m_{\pi\phi}$. At the region above the peak, the contribution of the $-g_{\mu\nu}$ term decreases more quickly than that of the $\frac{p^\mu p^\nu}{p^2}$ term, and then the $\frac{p^\mu p^\nu}{p^2}$ term becomes more important at higher $m_{\pi\phi}$. It is also interesting to note that because of the destructive effects between these two terms the ρ_{00}^{ϕ} drops faster in Model IV than in Model III. In particular, in Model IV with taking into account the K^*'s width the ρ_{00}^{ϕ} may approach 0 at about $m_{\pi\phi} = 1.50$ GeV.

Finally, to compare with experimental data, it is also necessary to estimate possible effects from the background contributions. Possible resonance contributions in the $\pi^0\eta$ channel, such as the $a_0(980)$'s contribution, are not considered, since they can, in principle, be eliminated by a kinematic cut on the $\pi^0\eta$ invariant mass. In this work, the background contribution is modeled by a contact term [Fig. 1(d)], for which we adopt the Lagrangian density [14,29],

$$\mathcal{L}_{\Psi\eta\pi\phi} = g_{ct}\Psi^\mu\phi_\mu\pi\eta. \tag{13}$$

Since the relative strength of the background contribution is not presented in the experimental paper, here we adjust the coupling constant g_{ct} to make the background contribution have the same magnitude as that of the resonance contribution or the triangle diagrams at the peak position in the invariant mass spectrum. In this way, the ρ_{00}^{ϕ} with including background contribution is calculated for various models and shown in Fig. 5.[2] In the region where the background term dominates the reaction, the value of ρ_{00}^{ϕ} approaches 0.33 corresponding to the pure background contribution (see short-dotted line in Fig. 4) for all models. At the peak position, the resonance or triangle diagram contribution has a similar strength as the background contribution as we suppose. For TS models, we find the ρ_{00}^{ϕ} is slightly reduced. For the $h_1(1415)$ production process (Model II), since the resonance production contribution and background term individually leads to a similar ρ_{00}^{ϕ}, we find the inclusion of the background contribution does not significantly change the ρ_{00}^{ϕ}. While for the C(1480) production process (Model I), the value of the ρ_{00}^{ϕ} is determined by a mix of the background and resonance contribution. In this case the ρ_{00}^{ϕ} always lies in a range between the values determined by the C(1480) contribution and background contribution solely, i.e., in a range from 0 to 0.33. Therefore, we find that although the inclusion of the background contribution could change the line shapes of ρ_{00}^{ϕ} for different models, the main difference between the TS models and resonance models remains and can be used to distinguish various mechanisms. In particular, the discrepancies between Model III and IV at higher $m_{\pi\phi}$ still exist and may offer the opportunity to distinguish these two models. However, since the contributions due to the TS mechanism become smaller at higher $m_{\pi\phi}$, it may be challenging to capture such discrepancies.

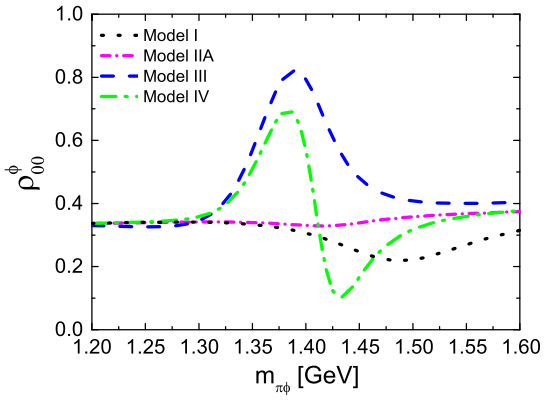

FIG. 5. The calculated ρ_{00}^{ϕ} for various models with including the background contribution. For Model III and Model IV, the finite width of K^* has been taken into account.

[2]In Fig. 5, we only show the results corresponding to the constructive interference case. For the triangle diagrams, we do not consider the destructive interference case, since in this case we cannot get a peak structure in the invariant mass spectrum, which is conflict with the experimental observation. For the resonance production process, we find the interference effects are insignificant and the results are similar in both constructive and destructive cases.

V. SUMMARY

In this work, we study the spin density matrix element ρ_{00}^{ϕ} of the ϕ in the reaction $J/\psi \to \eta\pi\phi$. We find that the ρ_{00}^{ϕ} shows distinct features when considering different reaction mechanisms, i.e., the production of a resonance or TS mechanism. According to our calculation results, it is found that the special kinematic conditions required by kinematic singularities and the properties of the involved vertex functions in the loop results in an enhancement of the ρ_{00}^{ϕ} near the TS. If the TS mechanism indeed plays an important role, we expect that the ρ_{00}^{ϕ} should take a relatively large value and have a peak versus the invariant mass $m_{\pi\phi}$ near the TS, which is absent for the resonance models. Therefore, by exploring the ρ_{00}^{ϕ} in this reaction it is possible to distinguish the various models and offer an alternative way to study the triangle singularity. Until now there is still no clear experimental evidence identifying the contribution of triangle singularity, it is then helpful to develop some new methods to distinguish various mechanisms. Although in this work we concentrate on the $J/\psi \to \eta\pi\phi$ reaction, it should be noted that the spin effects caused by the TS mechanism are general and can be exploited in other processes where the TS mechanism plays an important role and the spin states of final particles can be measured.

ACKNOWLEDGMENTS

We acknowledge Professor Feng-Kun Guo for his useful comments and suggestions. This work is partly supported by the National Natural Science Foundation of China under Grants No. U1832160 and No. 11375137, the Natural Science Foundation of Shaanxi Province under Grant No. 2019JM-025, and the Fundamental Research Funds for the Central Universities.

APPENDIX A: POLARIZATION VECTORS OF VECTOR MESON

Taking the polarization axis along the z axis, the polarization vectors for vector meson at rest are

$$\varepsilon_{+1}(\vec{p}=0)=\frac{-1}{\sqrt{2}}\begin{pmatrix}0\\1\\i\\0\end{pmatrix},\qquad \varepsilon_{-1}(\vec{p}=0)=\frac{1}{\sqrt{2}}\begin{pmatrix}0\\1\\-i\\0\end{pmatrix},$$
$$\varepsilon_{0}(\vec{p}=0)=\begin{pmatrix}0\\0\\0\\1\end{pmatrix}. \tag{A1}$$

For vector meson polarized along the direction with spherical angles (θ,ϕ) in its rest frame, the polarization vectors are obtained through

$$\begin{aligned}\varepsilon'_{\lambda}(\theta,\phi)&=\sum_{M}D_{M\lambda}(\phi,\theta,-\phi)\varepsilon_{M}\\&=e^{-i\phi\cdot 1}d^{1}_{1\lambda}(\theta)e^{i\phi\cdot\lambda}\varepsilon_{1}+e^{-i\phi\cdot 0}d^{1}_{0\lambda}(\theta)e^{i\phi\cdot\lambda}\varepsilon_{0}\\&\quad+e^{-i\phi\cdot(-1)}d^{1}_{-1\lambda}(\theta)e^{i\phi\cdot\lambda}\varepsilon_{-1}.\end{aligned} \tag{A2}$$

Then we can get

$$\varepsilon'_{+1}(\vec{p}=0)=\frac{-1}{\sqrt{2}}\begin{pmatrix}0\\\cos^2\frac{\theta}{2}-e^{2i\phi}\sin^2\frac{\theta}{2}\\i\left(\cos^2\frac{\theta}{2}+e^{2i\phi}\sin^2\frac{\theta}{2}\right)\\-e^{i\phi}\sin\theta\end{pmatrix}, \tag{A3}$$

$$\varepsilon'_{-1}(\vec{p}=0)=\frac{-1}{\sqrt{2}}\begin{pmatrix}0\\-\cos^2\frac{\theta}{2}+e^{-2i\phi}\sin^2\frac{\theta}{2}\\i\left(\cos^2\frac{\theta}{2}+e^{-2i\phi}\sin^2\frac{\theta}{2}\right)\\e^{-i\phi}\sin\theta\end{pmatrix}, \tag{A4}$$

$$\varepsilon'_{0}(\vec{p}=0)=\begin{pmatrix}0\\\sin\theta\cos\phi\\\sin\theta\sin\phi\\\cos\theta\end{pmatrix}. \tag{A5}$$

For taking a vector meson from rest to momentum p, the corresponding lorentz transformation matrix is defined as

$$\begin{pmatrix}p^0\\p^j\end{pmatrix}=\frac{1}{M_V}\begin{pmatrix}p^0 & p^i\\p^j & \frac{p^jp^i}{p^0+M_V}+\delta^{ji}M_V\end{pmatrix}\begin{pmatrix}M_V\\0\end{pmatrix}, \tag{A6}$$

where M_V represents the mass of the vector meson. So for a vector meson moving at the momentum p and polarized along (θ,ϕ), the polarization vectors are

$$\varepsilon_{\lambda}(p)=\frac{1}{M_V}\begin{pmatrix}\vec{p}\cdot\vec{\varepsilon}'_{\lambda}\\\vec{p}\,\frac{\vec{p}\cdot\vec{\varepsilon}'_{\lambda}}{p^0+M_V}+M_V\vec{\varepsilon}'_{\lambda}\end{pmatrix}. \tag{A7}$$

If the polarization axis of vector meson is taken along the direction of its three-momentum $\vec{p}$, i.e., the helicity state, it is clear that $\vec{\varepsilon}'_0$ is parallel with $\vec{p}$. So we can get $\vec{\varepsilon}'_0\times\vec{p}=0$. Furthermore, due to the relation $\vec{\varepsilon}'_{\lambda}\cdot\vec{\varepsilon}'_{\lambda'}=\delta_{\lambda\lambda'}$, we also have $\vec{\varepsilon}'_{\pm1}\cdot\vec{p}=0$. And then the helicity state of the vector meson can be rewritten as

$$\varepsilon_{\pm1}=\begin{pmatrix}0\\\vec{\varepsilon}'_{\pm1}\end{pmatrix},\qquad \varepsilon_0=\frac{1}{M_V}\begin{pmatrix}|\vec{p}|\\p^0\vec{\varepsilon}'_0\end{pmatrix}. \tag{A8}$$

APPENDIX B: PROPERTIES OF THE VPP AND VVP VERTICES

For the VPP vertex, we have the interaction Lagrangian

$$\mathcal{L}_{VPP} = g_{VPP} V_\mu (P_1 \partial^\mu P_2 - P_2 \partial^\mu P_1), \tag{B1}$$

and the corresponding vertex function is

$$\begin{aligned} -it_{V\to PP} &= g_{VPP}\varepsilon_\mu (p_1 - p_2)^\mu \\ &= g_{VPP}\varepsilon_\mu [p_1 - (p_V - p_1)]^\mu \\ &= 2 g_{VPP}\varepsilon \cdot p_1, \end{aligned} \tag{B2}$$

where p_1, p_2, and p_V represent momenta of the two pseudoscalar mesons and the vector meson V. If $\vec{p}_1$ and $\vec{p}_V$ are collinear in some reference frame, according to Eq. (A8) the helicity states of the vector meson have the property

$$\varepsilon_{\pm 1} \cdot p_1 = 0 \cdot p_1^0 - \overrightarrow{\epsilon'}_{\pm 1} \cdot \overrightarrow{p_1} = 0. \tag{B3}$$

Therefore in the reference frame where the three momenta p_1 and p_V are parallel, the VPP vertex has the property that the produced V meson can only be in the helicity state with $\lambda = 0$, which is a result of angular momentum conservation.

For the VVP vertex, the Lagrangian is written as

$$\mathcal{L}_{VVP} = g_{VVP}\epsilon^{\mu\nu\alpha\beta}\partial_\mu V_{1\nu}\partial_\alpha V_{2\beta}. \tag{B4}$$

The corresponding vertex function is

$$-it_{V_1\to V_2 P} = g_{VVP}\varepsilon_{\mu\nu\alpha\beta} p^\mu \varepsilon_1^\nu q^\alpha \varepsilon_2^{*\beta}, \tag{B5}$$

with p and q denoting the momentum of the vector mesons V_1 and V_2. ε_1 and ε_2 represent their corresponding polarization vectors. We can rewrite the vertex function in the following form:

$$\begin{aligned} -it_{V_1\to V_2 P} = g_{VVP}[&p^0(\vec{\varepsilon}_1 \times \vec{q})\cdot\vec{\varepsilon}_2^* - \varepsilon_1^0(\vec{p}\times\vec{q})\cdot\vec{\varepsilon}_2^* \\ &+ q^0(\vec{p}\times\vec{\varepsilon}_1)\cdot\vec{\varepsilon}_2^* - \varepsilon_2^{*0}(\vec{p}\times\vec{\varepsilon}_1)\cdot\vec{q}]. \end{aligned} \tag{B6}$$

This expression shows that, if the three-momenta of the three particles are collinear and the helicity of V_2 is 0, the vertex function should vanish due to the equations $\vec{p}\times\vec{q} = \vec{\varepsilon}_{2,\lambda=0}\times\vec{q} = \vec{\varepsilon}_{2,\lambda=0}\times\vec{p} = 0$ (see Appendix A). It means only the helicity states with $\lambda = \pm 1$ contribute, and the produced vector meson V_2 should have $\rho_{00} = 0$. When the vector meson V_1 has a vanishing momentum or the calculation is performed in its rest frame, similar arguments also hold. This property can be understood in the following way. Let us consider the process V_1 decaying to V_2 and P. In this case, due to the conservation of parity and angular momentum, the orbital angular momentum of the final two particles can only be 1. If we choose the z axis along the momentum of V_2 in the V_1's rest frame, the magnetic quantum number of the initial state V_1 (denoted as m) can only have the same value as the helicity of the V_2 (denoted as λ_2) due to the conservation of z-component of total angular momentum. In this case $\lambda_2 = 0$ is forbidden, because the coupling of the spin states of V_1 and V_2 ($|1,0\rangle$ and $|1,0\rangle$) with orbital angular momentum state $|1,0\rangle$ is vanishing due to the Clebsch-Gordan coefficient $\langle 10,10|10\rangle = 0$.

[1] M. Mikhasenko, B. Ketzer, and A. Sarantsev, Phys. Rev. D **91**, 094015 (2015).
[2] G. D. Alexeev *et al.* (COMPASS Collaboration), Phys. Rev. Lett. **127**, 082501 (2021).
[3] J. J. Xie, L. S. Geng, and E. Oset, Phys. Rev. D **95**, 034004 (2017).
[4] S. X. Nakamura, Phys. Rev. D **102**, 074004 (2020).
[5] E. Wang, J. J. Xie, W. H. Liang, F. K. Guo, and E. Oset, Phys. Rev. C **95**, 015205 (2017).
[6] X. H. Liu, G. Li, J. J. Xie, and Q. Zhao, Phys. Rev. D **100**, 054006 (2019).
[7] S. X. Nakamura, Phys. Rev. D **103**, L111503 (2021).
[8] F. K. Guo, C. Hanhart, Ulf-G. Meißner, Q. Wang, Q. Zhao, and B. S. Zou, Rev. Mod. Phys. **90**, 015004 (2018).
[9] F. K. Guo, X. H. Liu, and S. Sakai, Prog. Part. Nucl. Phys. **112**, 103757 (2020).
[10] M. Ablikim *et al.* (BESIII Collaboration), Phys. Rev. Lett. **108**, 182001 (2012).
[11] M. C. Du and Q. Zhao, Phys. Rev. D **100**, 036005 (2019).
[12] Y. Cheng and Q. Zhao, Phys. Rev. D **105**, 076023 (2022).
[13] M. C. Du and Q. Zhao, Phys. Rev. D **104**, 036008 (2021).
[14] Hao-Jie Jing, Shuntaro Sakai, Feng-Kun Guo, and Bing-Song Zou, Phys. Rev. D **100**, 114010 (2019).
[15] M. Ablikim *et al.* (BESIII Collaboration), Phys. Rev. Lett. **121**, 022001 (2018).
[16] S. I. Bityukov *et al.*, Phys. Lett. B **188**, 383 (1987).
[17] L. G. Landsberg, Sov. J. Nucl. Phys. **55**, 1051 (1992).
[18] M. C. Du, Y. Cheng, and Q. Zhao, Phys. Rev. D **106**, 054019 (2022).
[19] M. Tanabashi *et al.* (Particle Data Group), Phys. Rev. D **98**, 030001 (2018) and 2019 update.
[20] M. Ablikim *et al.* (BESIII Collaboration), Phys. Rev. D **98**, 072005 (2018).
[21] U.-G. Meissner, Phys. Rep. **161**, 213 (1988).
[22] L. Roca, E. Oset, and J. Singh, Phys. Rev. D **72**, 014002 (2005).

[23] P. Lichard and J. Juráň, Phys. Rev. D **76**, 094030 (2007).
[24] F. Murgia and M. Melis, Phys. Rev. D **51**, 3487 (1995).
[25] M. Jacob and G. C. Wick, Ann. Phys. (N.Y.) **7**, 404 (1959).
[26] K. Schilling, P. Seyboth, and G. E. Wolf, Nucl. Phys. **B15**, 397 (1970).
[27] S. H. Kim, Y. Oh, and A. I. Titov, Phys. Rev. C **95**, 055206 (2017).
[28] M. Bayar, F. Aceti, F. K. Guo, and E. Oset, Phys. Rev. D **94**, 074039 (2016).
[29] U. G. Meissner and J. A. Oller, Nucl. Phys. **A679**, 671 (2001).